

# Solid-state $S = 1$ spin centers with zero-field splitting as quantum simulators for $S = 1/2$ critical behavior

Troy Losey<sup>1</sup>, Denis R. Candido<sup>2</sup>, Y. Meurice<sup>2</sup>, M. E. Flatté<sup>2</sup>, S.-W. Tsai<sup>1</sup>, and Jin Zhang<sup>2\*</sup>

<sup>1</sup> Department of Physics and Astronomy, University of California, Riverside, California 92521, USA

<sup>2</sup> Department of Physics and Astronomy, University of Iowa, Iowa City, Iowa 52242, USA

(Dated: September 16, 2022)

In this work we propose a novel solid-state platform for creating quantum simulators based on implanted  $S = 1$  spin centers in semiconductors. We show that under the presence of an external magnetic field, an array of  $S = 1$  spin centers interacting through magnetic dipole-dipole interaction can be mapped into an effective spin-half system equivalent to the XYZ model in an external field. Interestingly, this system shows a wide range of phases and critical behaviors that can be obtained by changing both the magnetic field and the orientational displacement of the spin centers with respect to their main symmetry axis. Notably, our model contains a line where the system is in a critical floating phase that terminates at a Berezinskii-Kosterlitz-Thouless transition point and a Pokrovsky-Talapov transition point. It can also be tuned between an isotropic Heisenberg point and a transverse Ising universality class. We propose this system as the first quantum simulator for the floating phase with spin-centers in solid-state materials.

## I. INTRODUCTION

A rapidly expanding field of quantum information science is the creation of quantum simulators specifically designed for handling complex problems not solvable with classical computers. Critical phenomena present universal behavior that depend only on the symmetries and dimensionality of the system and provide unifying principles that applies across very different fields of physics. The robustness of the universal properties makes it promising that general principles and different universality classes of complex systems may be investigated and tested with specially designed quantum simulators that contain the essential physics and can be created and probed in the laboratory in a controlled way. Quantum spin chains have been extensively studied due to their relative simplicity and rich behavior. The physics of spin-half chains is particularly interesting and can be directly mapped to systems of fermions.

Most recently, defects in solids with spin (spin centers) have been demonstrating to be a promising platform for quantum information science due to their many applications [1–6]. These spin centers can be optically initialized and read, and present long spin coherence time even at room temperature. Additionally, due to the sensitivity of their energy levels to both magnetic and electric fields, they are also great candidates for quantum sensing and metrology [7–25]. Many different examples of solid-state spin centers have been emerging in the last years, e.g., the negatively-charged nitrogen-vacancy (NV) [3, 4, 26] and silicon-vacancy (SiV) [27–30] spin centers in diamond; and divacancy spin centers in silicon carbide (SiC) [31–34]. Most recent advances on the spatial precision for the implantation of these spin centers [35, 36] allows for the corresponding creation of room-temperature coher-

ent interacting spin chains [37–40]. Interestingly, the interaction between these spins can be controlled through the relative position of the spin centers within the crystal, in addition to applied external magnetic and electric fields. Moreover, as crystal hosts are much larger than the typical spin-spin implantation separation, scalability of these spin chains appears feasible. Therefore, spin chains made of spin centers become a promising alternative solid state candidate for the implementation of quantum simulators.

Accordingly, in this paper, we exploit the remarkable recent advances in the creation and control of spin defects, and propose a solid-state quantum simulator for a spin-half system. Interestingly, we show that this system presents a number of different phases and different critical behaviors, which can be controlled for different arrangements of spin centers and values of the magnetic field. More specifically, an external magnetic field is used to create an effective  $S = 1/2$  system with various spin-spin interaction terms. The phase diagram for this  $S = 1/2$  system contains a critical line that corresponds to the isotropic Heisenberg model, critical lines that correspond to floating phases, Pokrovsky-Talapov (PT) [41] points, transverse Ising transitions and the gapped phases. A Berezinskii-Kosterlitz-Thouless (BKT) point is also expected at the point separating the floating phase and gapped phase. The presence of the floating phase makes the quantum simulator we propose here a promising potential candidate to study emerging incommensurate order and associated critical behavior.

The paper is organized as follows. In Section II, we start by introducing the general Hamiltonian that describes spin centers, followed by a discussion of the dipole-dipole coupling, and of the projection of the Hamiltonian onto an effective spin-half subspace. We then consider material candidates where this quantum simulator can be realized. In Section III, we present our results and discuss the most interesting regions of the phase diagram. The phase diagram can be parameterized

\* jin-zhang@uiowa.edu

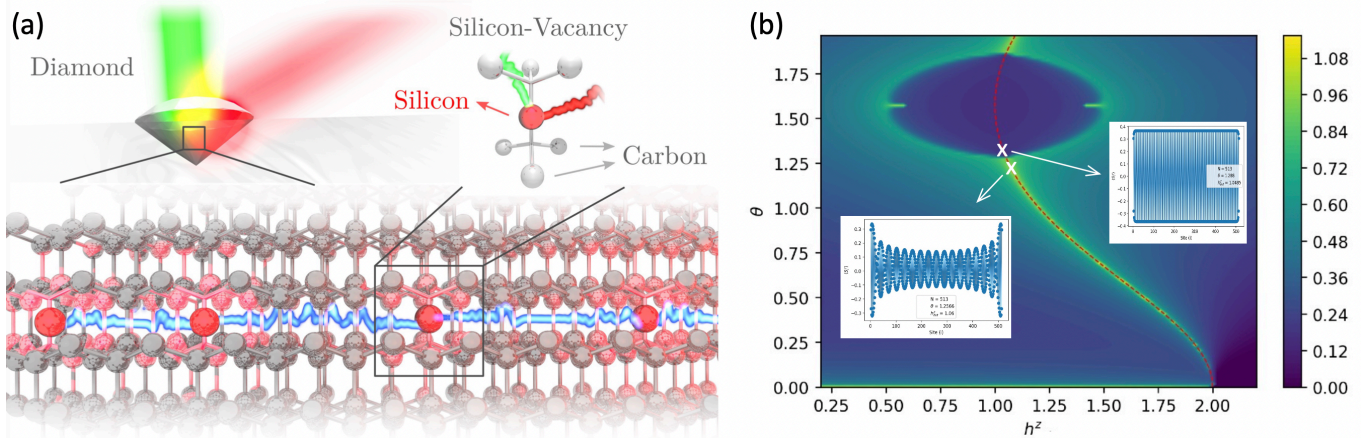


FIG. 1. (a) Schematic representation of Silicon-Vacancy in Diamond and the corresponding spin chain of SiVs coupled through dipole-dipole interaction. (b) The phase diagram of the effective spin-half SiV chain, demonstrated by the contour plot of von Neumann entanglement entropy  $S_{vN}$ . The phase boundaries are indicated by the peaks of  $S_{vN}$ . The circle is an Ising critical line, and the bright yellow curve connecting the PT point on the circle and the PT point at  $(\theta = 0, h^z = 2)$  coincides with the  $\Gamma_x = 0$  line (red dashed line) of the rotated Hamiltonian in Eq. (10), which stays in a critical floating phase near the PT points and goes into a gapped phase via BKT transitions for  $0.15 \lesssim \theta \lesssim 0.8$ . The insets show the spin density profiles for the AFM phase inside the circle at  $\theta = 0.41\pi$  and the incommensurate critical floating phase at  $\theta = 0.4\pi$  on the  $\Gamma_x = 0$  line.

by an angle  $\theta$  defined as the angle between the crystal axial direction and the alignment direction of the chain of spin centers.

## II. SOLID-STATE SPIN CENTER IMPLEMENTATION FOR QUANTUM SIMULATORS

In this section we establish a novel way for implementing quantum simulators in solid-state platforms. Our new proposal relies on the use of the spin center in semiconductors for creating interacting spin chain models in solid-state systems. Accordingly, we first provide the Hamiltonian for the spin centers, and for the dipole-dipole interaction between them. We then discuss different spin center candidates for the implementation. Finally, we show that the total Hamiltonian can be mapped into a spin-1/2 XYZ chain with an applied magnetic field along  $x$ - and  $z$ -direction.

### A. Spin center Hamiltonian

The Hamiltonian for the ground state of spin centers in solids can be generally described by a zero-field splitting term, plus the Zeeman interaction, namely

$$\mathcal{H}_S = h\mathbf{S} \cdot \mathbf{D} \cdot \mathbf{S} + h\mathbf{B}(\mathbf{r}) \cdot \frac{\gamma}{2\pi} \cdot \mathbf{S}, \quad (1)$$

where  $h$  is Planck's constant,  $\mathbf{D}$  is the zero-field splitting tensor arising from spin-spin interaction [26],  $\gamma/2\pi$

is the gyromagnetic (or g-factor) tensor,  $\mathbf{S}$  is the spin-center spin, and  $\mathbf{B}(\mathbf{r})$  is the magnetic field at the position of the spin-center,  $\mathbf{r}$ . For highly-symmetric spin centers, e.g., NV<sup>-1</sup>-center in diamond, (hh) and (kk) divacancies in SiC, and SiV<sup>0</sup> in diamond, the low-energy effective Hamiltonian is described as arising mainly from two interacting electrons that form a triplet manifold  $\{|0\rangle, | -1\rangle, |1\rangle\}$  with Hamiltonian

$$\mathcal{H}_S = hD(S^z)^2 + \frac{h\gamma}{2\pi}\mathbf{B}(\mathbf{r}) \cdot \mathbf{S}, \quad (2)$$

where  $D$  is the zero-energy splitting between the triplet states  $m = 0$  ( $|0\rangle$ ) and  $m = \pm 1$  ( $| \pm 1\rangle$ ), and  $S_x$ ,  $S_y$ , and  $S_z$  are the triplet spin-1 matrices. Although spin centers also possess excited states, those are separated by relatively higher energy (100 THz) compared to the energy scale associated to the ground state (1 GHz), and accordingly, will be neglected in this work. Accordingly, in the presence of an external magnetic field along the  $z$ -direction,  $\mathbf{B} = B\hat{z}$ , the triplet energy levels read

$$E_{m=\pm 1} = hD \pm \frac{h\gamma}{2\pi}B, \quad (3)$$

$$E_{m=0} = 0. \quad (4)$$

For the majority of spin centers,  $D \sim 1$  GHz and  $\gamma/2\pi \sim 28$  GHz/T, thus showing that spin centers can be easily manipulated with microwave frequency, and also respond sensitively to an external magnetic field.

## B. Magnetic dipole-dipole coupling between pin centers

If we now consider an array of spin centers separated by inter-atomic distances, different spin centers will be coupled to each other through both magnetic dipole-dipole coupling, and exchange interaction. While the exchange interaction dominates for inter-atomic distances  $d \lesssim 2$  nm [42, 43], the dipole-dipole dominates for  $d \gtrsim 5$  nm. Assuming a chain with spin centers separated by distances  $\gtrsim 10$  nm, we can disregard the exchange, yielding for the effective interacting Hamiltonian between spin centers  $i$  and  $j$ ,

$$\mathcal{H}_{\text{int}}^{ij} = \frac{\mu_0(h\gamma/2\pi)^2}{4\pi|\mathbf{r}_{ij}|^3} [3(\mathbf{S}_j \cdot \hat{\mathbf{r}}_{ij})(\mathbf{S}_i \cdot \hat{\mathbf{r}}_{ij}) - (\mathbf{S}_j \cdot \mathbf{S}_i)], \quad (5)$$

where  $\mu_0$  is the vacuum permeability,  $\mathbf{r}_{ij}$  is the displacement vector between spins  $i$  and  $j$ , and  $\hat{\mathbf{r}}_{ij} = \mathbf{r}_{ij}/|\mathbf{r}_{ij}|$ . In this paper, the  $z$ -axis is defined by the orientation of the spin center, pre-defined by the zero-field splitting term proportional to  $S_z$  within Eq. (2). Here, we express  $\mathbf{r}$  in spherical coordinates with corresponding angles  $\theta$  and  $\phi$ . Assuming that the  $z$ -axis of every spin center are aligned, our system possess azimuthal symmetry and we set  $\phi = 0$ . With these assumptions, we can conveniently write the magnetic dipole-dipole interaction between two spin centers  $i$  and  $j$  [Eq. (5)] as

$$\mathcal{H}_{\text{int}}^{ij} = \frac{\mu_0(h\gamma/2\pi)^2}{4\pi|\mathbf{r}_{ij}|^3} [S_i^x \ S_i^y \ S_i^z] \cdot \mathbf{T} \cdot \begin{bmatrix} S_j^x \\ S_j^y \\ S_j^z \end{bmatrix}, \quad (6)$$

with dipole-dipole tensor

$$\mathbf{T} = \begin{bmatrix} 3\sin^2(\theta) - 1 & 0 & \frac{3}{2}\sin(2\theta) \\ 0 & -1 & 0 \\ \frac{3}{2}\sin(2\theta) & 0 & 3\cos^2(\theta) - 1 \end{bmatrix}. \quad (7)$$

Assuming typical electronic gyromagnetic ratio ( $\gamma/2\pi \sim 28$  GHz/T) and  $|\mathbf{r}_{ij}| \sim 10$  nm, we obtain  $\mathcal{H}_{\text{int}}^{ij}/h \sim 50$  kHz, which is shown to be much stronger than the dephasing and relaxation rates of spin centers [6].

Considering a spin chain of equally spaced ( $|\mathbf{r}_{ij}| = |\mathbf{r}|$ )  $N$  spin centers oriented along a straight line, and assuming only nearest-neighbor interactions due to the short-range character of the dipole-dipole interaction, we obtain

$$\mathcal{H}_{\text{tot}} = \sum_i \mathcal{H}_{S_i} + \sum_{i,j} \mathcal{H}_{\text{int}}^{ij} \delta_{i,j \pm 1}. \quad (8)$$

## C. Projection onto a spin-half manifold

Despite the spin-1 character of our spin centers, we can effectively map the total spin-1 interacting Hamiltonian [Eq. (8)] into a spin-1/2 interacting Hamiltonian. To do so, we first apply a magnetic field  $\mathbf{B} = B_c \hat{z}$  with  $B_c \sim D/(\gamma/2\pi)$ , such that the levels  $| -1 \rangle$  and  $| 0 \rangle$  are

nearly degenerate. Under this condition, the state  $| 1 \rangle$  is separated from both  $| -1 \rangle$  and  $| 0 \rangle$  by  $\sim 1$  GHz. As the coupling between different spin centers is  $\sim 50$  kHz, non-degenerate perturbation theory guarantees that the effect of level  $| 1 \rangle$  within the manifold spanned by  $| -1 \rangle$  and  $| 0 \rangle$  can be neglected. Accordingly, by projecting the total spin-1 interacting Hamiltonian Eq. (8) onto the low energy  $\{| -1 \rangle, | 0 \rangle\}$  subspace, we obtain the spin-1/2 interacting Hamiltonian

$$H = J \sum_{i=1}^{N-1} \left\{ [3\sin^2(\theta) - 1] \sigma_i^x \sigma_{i+1}^x - \sigma_i^y \sigma_{i+1}^y \right. \\ \left. + \frac{3\cos^2(\theta) - 1}{2} \sigma_i^z \sigma_{i+1}^z + \frac{3\sin(2\theta)}{2\sqrt{2}} (\sigma_i^x \sigma_{i+1}^z + \sigma_i^z \sigma_{i+1}^x) \right\} \\ - J \sum_{i=1}^N \left[ (h^z + 3\cos^2(\theta) - 1) \sigma_i^z + \frac{3\sin(2\theta)}{\sqrt{2}} \sigma_i^x \right], \quad (9)$$

with  $J = 4\mu_0(h\gamma/2\pi)^2/4\pi|\mathbf{r}|^3$ ,  $h^z = (E_{m=0} - E_{m=-1})/J$  and Pauli matrices  $\sigma_{x,y,z}$  defined as  $\sigma_{\pm} = (\sigma_x + i\sigma_y)/2 = | -1 \rangle \langle 0 |$ . From now on, we will set  $J = 1$ .

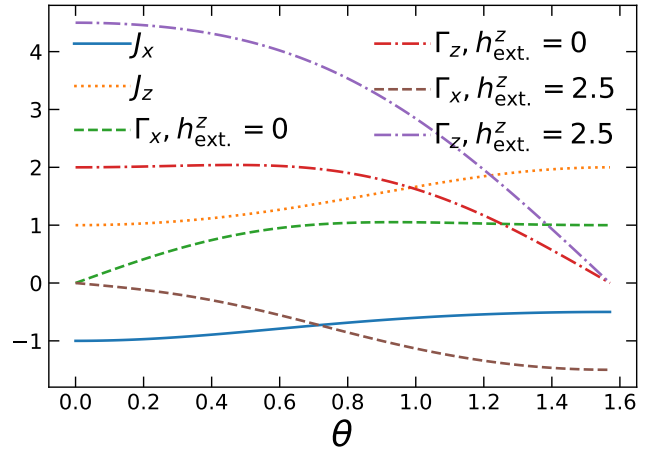


FIG. 2. The dependence of the coupling constants of the rotated Hamiltonian on  $\theta$ .

The Hamiltonian in Eq. (9) is invariant under the transformation  $\theta \rightarrow \theta + \pi/2$ , thus we restrict our analysis to  $\theta \in [0, \pi/2]$  in the following calculations. We set  $A = 3\sin^2(\theta) - 1$ ,  $B = [3\cos^2(\theta) - 1]/2$ ,  $C = 3\sin(2\theta)/(2\sqrt{2})$  and then rotate the system around the  $y$  axis by an angle  $\alpha$ . Choosing proper values of  $\alpha$  can eliminate the  $\sigma_i^x \sigma_{i+1}^z + \sigma_i^z \sigma_{i+1}^x$  terms, yielding the following XYZ model

$$\tilde{H} = \sum_i (J_x \sigma_i^x \sigma_{i+1}^x + J_z \sigma_i^z \sigma_{i+1}^z - \sigma_i^y \sigma_{i+1}^y) \\ - \sum_i (\Gamma_z \sigma_i^z + \Gamma_x \sigma_i^x), \quad (10)$$

with an external magnetic field along the  $x$  and  $z$  direc-

tions,  $\Gamma_z$  and  $\Gamma_x$ , respectively. We have also defined

$$J_{x(z)} = \mp \sqrt{\frac{(A-B)^2}{4} + C^2 + \frac{A+B}{2}}, \quad (11)$$

$$\Gamma_z = (h^z + 2B) \cos(\alpha) + 2C \sin(\alpha) \quad (12)$$

$$\Gamma_x = -(h^z + 2B) \sin(\alpha) + 2C \cos(\alpha) \quad (13)$$

$$\alpha = \begin{cases} \frac{1}{2} \arctan \left( \frac{2C}{B-A} \right), & \text{if } 0 \leq \theta < \arcsin(\frac{2}{3}) \\ \frac{\pi}{4}, & \text{if } \theta = \arcsin(\frac{2}{3}) \\ \frac{1}{2} \arctan \left( \frac{2C}{B-A} \right) + \frac{\pi}{2}, & \text{if } \arcsin(\frac{2}{3}) < \theta \leq \frac{\pi}{2} \end{cases} \quad (14)$$

Fig. 2 shows the coupling constants as functions of  $\theta$ . At  $\theta = 0$ ,  $J_x = -1$ ,  $J_z = 1$ , and  $\Gamma_x = 0$ , after a rotation around  $z$  axis by  $\pi$  for even or odd sites, the Hamiltonian is a Heisenberg model in an external field along the  $z$ -direction. From  $\theta = 0$  to  $\theta = \pi/2$ ,  $J_z$  increases from 1 to 2 and  $J_x$  increases from  $-1$  to  $-1/2$ . At  $\theta = \pi/2$ ,  $\Gamma_z = 0$ ,  $J_z$  dominates the interactions so the Hamiltonian should have an Ising transition as the transverse Ising model does. There are two special lines corresponding to  $\Gamma_x = 0$  and  $\Gamma_z = 0$ , respectively. On each line,  $h^z$  is fixed and the Hamiltonian only depends on  $\theta$ . The external fields on the two lines are determined by the following equations

$$\Gamma_z = 2C/\sin(\alpha) \text{ for } \Gamma_x = 0 \quad (15)$$

$$\Gamma_x = 2C/\cos(\alpha) \text{ for } \Gamma_z = 0 \quad (16)$$

#### D. Spin center candidates

Here we explore, discuss and assess the best spin center candidates for realizing our proposal. As already mentioned, there are many examples for spin-1 spin centers in solid-state systems relevant for our proposal, including the different (hh), (kk), (hk) and (kh) di-vacancies in SiC, and both NV<sup>-1</sup> and SiV in diamonds.

Within this candidates, the one that is more established in terms of understanding, knowledge, control, implantation precision and manipulation is the NV<sup>-1</sup> center in diamonds. However, the majority of the Nitrogen isotopes, <sup>14</sup>N and <sup>15</sup>N, respectively, have a nuclear spin. Since the spin of the NV<sup>-1</sup> centers are close to the N atoms, the hyperfine interaction between the electronic spin and nuclear spin is substantial, with corresponding strength  $\gtrsim 2$  MHz [26, 44, 45]. As the magnetic dipole-dipole interaction produces NV-NV coupling around  $\sim 50$  kHz, this coupling would be suppressed by the coupling of the NV to the N nuclear spin.

Due to the reason mentioned previously, the realization of our proposal will be optimal for solid-state systems that do not present strong hyperfine interaction between spin centers and non-zero spin nuclei. Accordingly, both di-vacancies in SiC and SiV in diamond are shown to be better spin center candidates for our proposal as the majority of their atoms (Si and C) does not have nuclear spin. We emphasize that although <sup>12</sup>C have zero nuclear spin, <sup>13</sup>C has not. However, the latter only represent  $\sim 1\%$  of the whole Carbon atoms of the crystal, and

accordingly, is not expected to suppress the dipole-dipole interaction.

### III. RESULTS

We perform finite-size density-matrix renormalization group (DMRG) calculations [46–48] with ITENSOR JULIA LIBRARY [49]. We gradually increase the bond dimension during the variational sweeps until the truncation error is below  $10^{-10}$ . Some high-precision calculations using a truncation error of  $10^{-11}$  are specified below. DMRG sweeps are terminated once the ground-state energy changes less than  $10^{-11}$  and the von Neumann entanglement entropy changes less than  $10^{-8}$  in the last two sweeps. All results use open boundary conditions (OBCs) unless otherwise stated. We use the peak of von Neumann entanglement entropy  $S_{vN}$  as the phase-transition indicator. Dividing the system into two parts,  $\mathcal{A}$  and  $\mathcal{B}$ , the entanglement entropy between  $\mathcal{A}$  and  $\mathcal{B}$  is

$$S_{vN} = -\text{Tr}[\hat{\rho}_{\mathcal{A}} \ln(\hat{\rho}_{\mathcal{A}})], \quad (17)$$

where  $\hat{\rho}_{\mathcal{A}} = \text{Tr}_{\mathcal{B}}\langle \Psi_0 | \Psi_0 \rangle$  is the reduced density matrix for block  $\mathcal{A}$  in the ground state  $|\Psi_0\rangle$ . At a critical point, conformal field theory (CFT) predicts that the entanglement entropy diverges logarithmically with the system size [50, 51]

$$S_{vN} = -\frac{c}{6} \ln N + s_0, \quad (18)$$

where  $c$  is the central charge, and  $s_0$  is a non-universal constant.

Figure 1(b) shows the phase diagram of the model in  $\theta$ - $h^z$  plane. At  $\theta = 0$ , the system is a Heisenberg model in an external field along  $z$ -direction and  $\Gamma_z = 2 + h^z$ . According to the results in Refs. [52, 53], the model is in the critical partially magnetized (PM) phase for  $\Gamma_z \in (0, 4)$ , and goes to the fully magnetized (FM) phase for  $\Gamma_z > 4$  via a Pokrovsky-Talapov (PT) transition at  $\Gamma_z = 4$  ( $h^z = 2$ ). Close to  $\theta = \pi/2$ , there is a circular Ising critical line centered at  $\theta = \pi/2, h^z = 1$ , inside which is an antiferromagnetic (AFM) phase in  $z$ -direction, and outside which is a disordered phase. A line of entanglement peak connects the circle and the point  $(\theta = 0, h^z = 2)$ , which corresponds to the line determined by  $\Gamma_x = 0$ . Both ends of the line are PT transition points, which are the boundary of the critical floating phase. On this line, the floating phase emerges from the upper PT point down to  $\theta \approx 0.8$  and from the bottom PT point up to  $\theta \approx 0.15$ . For  $0.15 \lesssim \theta \lesssim 0.8$  on the line, the system goes into a gapped phase via two Berezinskii-Kosterlitz-Thouless (BKT) transitions. In the following, we analyse the critical properties of these phase transitions.

### A. $\theta = 0$

The Hamiltonian for  $\theta = 0$  is

$$H_{\theta=0} = \sum_i (-\sigma_i^x \sigma_{i+1}^x - \sigma_i^y \sigma_{i+1}^y + \sigma_i^z \sigma_{i+1}^z) - (h^z + 2) \sum_i \sigma_i^z. \quad (19)$$

The SU(2) Heisenberg point is at  $h^z = -2$ , which is a BKT critical point with a central charge  $c = 1$ . As we increase  $h^z$ , a nonzero magnetization in  $z$ -direction is induced. As the total magnetization is conserved, it increases discontinuously and the system is in the PM phase. When  $h^z$  is large enough, all the spins are along  $z$ -direction, the magnetization reaches maximum and the system is in the FM phase. This feature results in oscillations in the entanglement entropy. As shown in Fig. 3, the fluctuating entanglement entropy remains high in the PM phase at  $h^z < 2$ , indicating that the PM phase is critical. When it approaches the FM phase, the entanglement entropy suddenly jumps to zero.

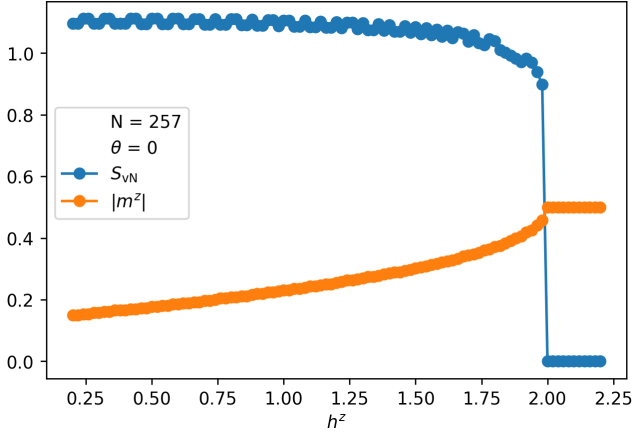


FIG. 3. The entanglement entropy and the magnetization as a function of  $h^z$  at  $\theta = 0$  for  $N = 257$ . The high entanglement regime is the PM phase and the low entanglement regime is the FM phase. The oscillations come from discontinuous change of total magnetization.

In the thermodynamic limit, the magnetization density along  $z$ -direction ( $m^z$ ) changes continuously with  $h^z$ , thus there is a power-law scaling for  $m^z$  near the phase transition inside the PM phase. In Fig. 4, we show the magnetization density as a function of  $h^z$  near  $h_c^z = 2$ . Assuming  $m^z \sim (h_c^z - h^z)^\beta$ , we obtain  $\beta = 0.48$  from a curve fit. The transition between the incommensurate PM phase and the commensurate FM phase should belong to the PT universality class that has  $\beta = \nu = 1/2$ . Our numerical result is consistent with this expectation.

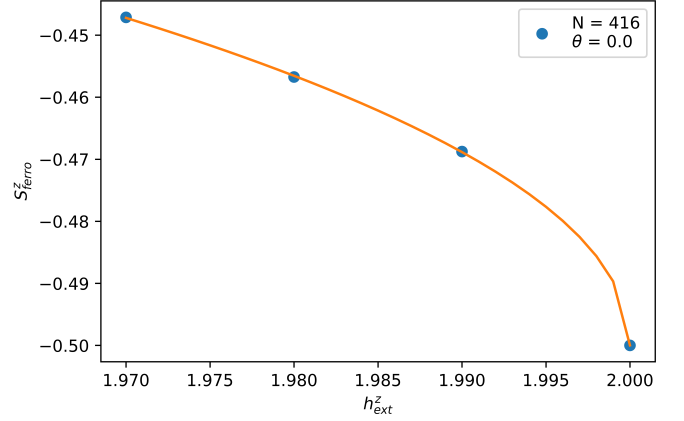


FIG. 4. The magnetization as a function of  $h^z$  near the phase transition point. Results are for  $N = 416$  sites. The power law fitting  $m^z \sim (h_c^z - h^z)^\beta$  gives  $\beta = 0.480$ .

### B. Ising circle

At  $\theta = \pi/2$ , the Hamiltonian becomes

$$H_{\theta=\frac{\pi}{2}} = \sum_i \left( -\frac{1}{2} \sigma_i^x \sigma_{i+1}^x - \sigma_i^y \sigma_{i+1}^y + 2\sigma_i^z \sigma_{i+1}^z \right) + (h^z - 1) \sum_i \sigma_i^x, \quad (20)$$

where  $J_z = 2|J_y| = 4|J_x|$  and  $\Gamma_z = 0$ , the dominant part of the model is a transverse Ising model, and we expect the phase transition to belong to the Ising universality class. Fig. 5(a) shows the extrapolation procedure to find the critical point  $h_c^z$ , where the peak positions of entanglement entropy at finite  $N$  is fit to a polynomial of  $1/N$ . The extrapolated value of  $h_c^z$  is 0.5036. We then calculate the entanglement entropy with different  $N$  at  $h_c^z$  and fit them with the expected scaling predicted by CFT in Eq. 18. The results are presented in Fig. 5(b) and the fitted value of  $c = 0.498$ , consistent with the value  $c = 0.5$  for Ising CFT.

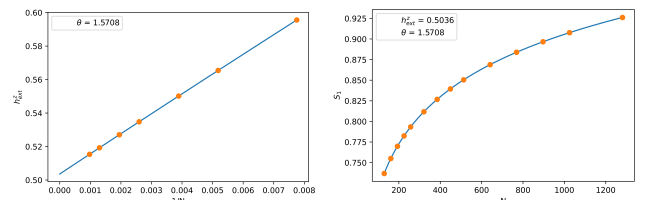


FIG. 5. Left: Extrapolation procedure for the peak position of the entanglement entropy at  $\theta = \pi/2$ . A polynomial fit gives the critical point  $h_c^z = 0.5036$ . Right:  $S_{VN}$  as a function of  $N$  at  $h_c^z$ . A logarithmic scaling fit gives  $c = 0.498$ .

We also check the results for  $\theta = 1.4$  and obtain  $h_c^z = 0.6298, c = 0.499$ . On the circular phase boundary,  $\theta$  is close to  $\pi/2$  and  $J_z$  is always the largest coupling constant, so all the points on the circle should be Ising

critical points. In Fig. 6, the staggered magnetization in  $z$ -direction  $m_{stag}^z = [\sum_i (-1)^i S_i^z]/N$  is presented. One can see that  $m_{stag}^z$  is nonzero inside the circle and zero outside the circle. Thus inside the circle, it is an AFM phase associated with transverse Ising model.

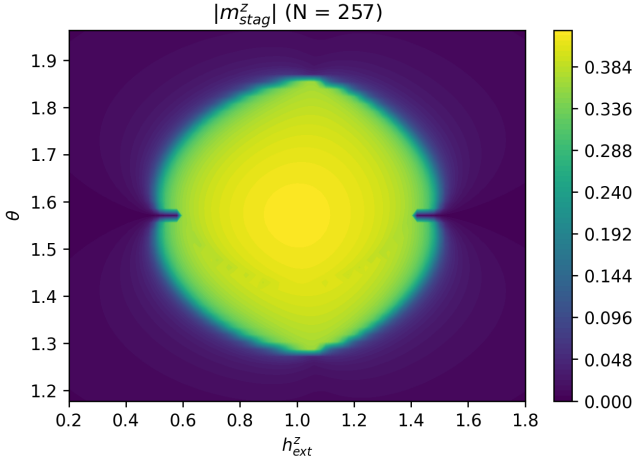


FIG. 6. The magnitude of the staggered magnetization in  $z$  direction  $|m_{stag}^z|$  for  $N = 257$  sites.

### C. $\Gamma_x = 0$ line

The  $\Gamma_x = 0$  line is special because a small field in  $x$  direction will reduce the symmetry of the XYZ model in an external field along  $z$ -direction. Thus the entanglement entropy should have a peak at  $\Gamma_x = 0$ . As shown in Fig. 1, the  $\Gamma_x = 0$  line connects the circular phase boundary to the PT point at  $\theta = 0$ . Based on Luttinger-liquid theory, the PT transition happens where the velocity becomes zero and the dispersion relation becomes quadratic, and the BKT transition happens where the Luttinger-liquid parameter is too large to stabilize the liquid phase. Thus there must be a critical floating phase near the PT point at  $\theta = 0$ , similar to the XY model in an external field along  $x$ -direction that is dual to the quantum ANNNI model and has a critical floating phase enclosed by a BKT line and a PT line [54].

However, we find that the entanglement entropy saturates at large enough  $N$  for  $\theta = 0.19$  and  $\theta = 0.5$  on the  $\Gamma_x = 0$  line. There must be a BKT transition around  $\theta = 0.15$  from the floating phase to a gapped phase as we increase  $\theta$ . To investigate the criticality at larger  $\theta$ , we study the entanglement scaling at  $\theta = 1.2$  in Fig. 7 and we find  $c = 1.02$ , consistent with the value in Gaussian CFT. Thus the system becomes critical again via another BKT transition as we further increase  $\theta$ . This BKT point is found to be around  $\theta = 0.8$ . A feature of the floating phase is that the spin density profile exhibits a wave with the wave vector changing continuously with the coupling constant. The inset of Fig. 1(b) and Fig. 7(b) present two

spin density profiles for  $\theta = 0.4\pi$  and  $\theta = 0.39\pi$ , respectively. One can see that the wave length at  $\theta = 0.39\pi$  is smaller than that at  $\theta = 0.4\pi$ . At the  $\Gamma_x = 0$  line but inside the circle, it is a commensurate AFM phase, thus the phase transition point on the circle should be another PT point. Notice that the entanglement entropy suddenly drops as the  $\Gamma_x = 0$  line crosses the circle. This behavior clearly distinguishes the PT point from a BKT point, where the entanglement entropy changes smoothly across the transitions.

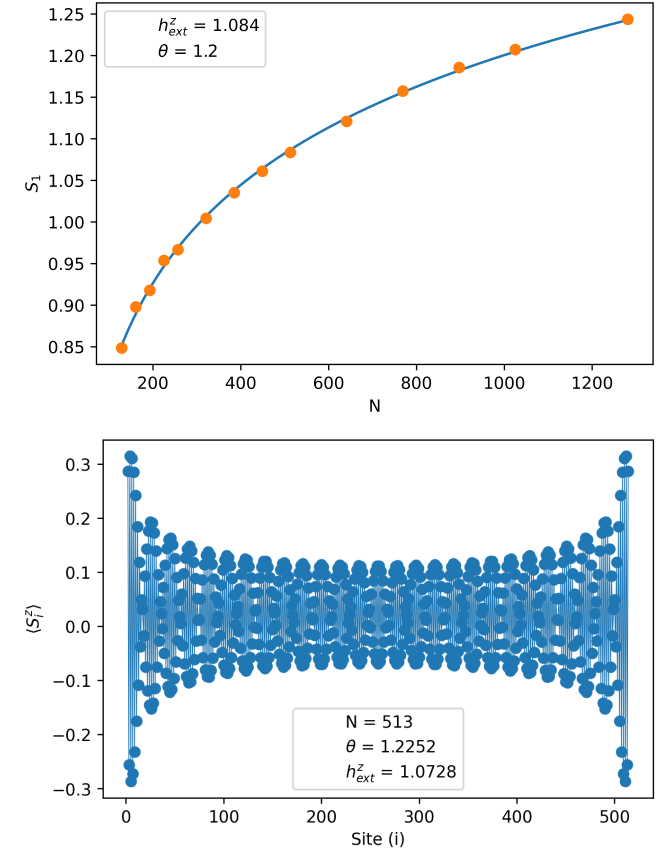


FIG. 7. Upper: Entanglement entropy  $S_{VN}$  as a function of  $N$ ,  $c = 1.02$  from the fit. Lower: Expectation value of  $\langle S_i^z \rangle$  at each site  $i$  in the critical floating phase at  $\theta = 1.2252$ .

## IV. CONCLUSIONS

We have proposed a quantum simulator for  $S = 1/2$  quantum critical behavior based on spin centers in SiC or diamond that can be arranged in a linear array. An external magnetic field can be used to project the  $S = 1$  Hamiltonian onto a sub-space governed by an effective  $S = 1/2$  Hamiltonian. This  $S = 1/2$  quantum simulator can be tuned with the external field and with the angle  $\theta$  between the direction of the spin-center array and the crystal axis. When  $\theta = 0$ , the quantum simulator gives the isotropic Heisenberg model in the presence of a

field. In the vicinity of  $\theta = \pi/2$ , the phases and critical behavior are described by the transverse Ising model universality class. In between these regimes, there is a line of enhanced entanglement entropy that present a number of interesting behavior, namely Pokrovsky-Talapov points, BKT points and critical floating phases characterized by incommensurate spin density wave. There have been much interest in realizing floating phases and in studying commensurate-to-incommensurate phase transitions[55–57], with proposals[58] for observing them in experiments with Rydberg arrays[59]. This is the first proposal of a quantum simulator for realizing floating phases that is based on spin-centers in solid state materials.

We have shown here that a large number of critical phenomena can be studied with  $S = 1$  spin-center arrays by projecting onto an effective  $S = 1/2$  Hamiltonian. It is worth noting that  $S = 1$  chains present many interesting phases and critical behaviors. Effective spin models with spin- $S$  were also proposed as quantum simulators for lattice field theories such as the O(2) model[60, 61] and the Abelian-Higgs model in (1+1)-dimensions[62–64]. The  $S = 1$  case represents a particularly interesting truncation of this quantum simulator[65, 66], and therefore spin-center arrays may be promising candidates as quantum simulators for these systems as well.

## ACKNOWLEDGMENTS

This work was supported in part by the National Science Foundation (NSF) RAISE-TAQS under Award Number 1839153 (S.W.T.), by the U.S. Department of Energy (DOE), Office of Basic Energy Sciences under Award Number DE-SC0019250 (M. E. F.) for the NV Hamiltonian derivation and DE-SC0019139 (Y.M.) for using quantum spin chains as quantum simulators. Computations were performed using the computer clusters and data storage resources of the UCR High Performance Computing Center (HPCC), which were funded by grants from NSF (MRI-1429826) and NIH (1S10OD016290-01A1).

## Appendix A: The effective spin-1/2 Hamiltonian from spin centers

In the NV centers, if the levels  $| -1 \rangle$  and  $| 0 \rangle$  are nearly degenerate, to the first-order approximation, we just need to keep the submatrix elements of spin-1 operators associated with the two states, then  $S_{S=1}^x \rightarrow \sqrt{2}S_{S=1/2}^x$ ,  $S_{S=1}^y \rightarrow \sqrt{2}S_{S=1/2}^y$ , and  $S_{S=1}^z \rightarrow S_{S=1/2}^z - 1/2$ . The

effective spin-1/2 Hamiltonian is

$$\begin{aligned} \frac{H}{J} = & \sum_{i=1}^{N-1} \left\{ [3 \sin^2(\theta) - 1] S_i^x S_{i+1}^x - S_i^y S_{i+1}^y \right. \\ & + \frac{3 \cos^2(\theta) - 1}{2} \left( S_i^z S_{i+1}^z + \frac{1}{4} \right) \\ & \left. + \frac{3 \sin(2\theta)}{2\sqrt{2}} (S_i^x S_{i+1}^z + S_i^z S_{i+1}^x) \right\} \\ & - \sum_{i=1}^N \left[ \frac{h_{ex}^z + 3 \cos^2(\theta) - 1}{2} S_i^z + \frac{3 \sin(2\theta)}{2\sqrt{2}} S_i^x + \frac{h_{ex}^z}{4} \right] \\ & + \left[ \frac{3 \cos^2(\theta) - 1}{4} (S_1^z + S_N^z) + \frac{3 \sin(2\theta)}{4\sqrt{2}} (S_1^x + S_N^x) \right] \end{aligned} \quad (\text{A1})$$

After leaving out the boundary terms and the constants, which do not change the criticality, and replacing the spin-1/2 operators by Pauli matrices, we obtain Eq. (9).

## Appendix B: Rotation of the spin-1/2 Hamiltonian

Rotating the system around  $y$  axis by an angle  $\alpha$ , the new spin operators change as follows

$$\sigma^x \rightarrow e^{is^y \alpha} \sigma^x e^{-is^y \alpha} = \cos(\alpha) \sigma^x + \sin(\alpha) \sigma^z \quad (\text{B1})$$

$$\sigma^z \rightarrow e^{is^y \alpha} \sigma^z e^{-is^y \alpha} = \cos(\alpha) \sigma^z - \sin(\alpha) \sigma^x \quad (\text{B2})$$

Then the new Hamiltonian can be written as

$$\begin{aligned} \tilde{H} = & \sum_i (J_x \sigma_i^x \sigma_{i+1}^x + J_z \sigma_i^z \sigma_{i+1}^z - \sigma_i^y \sigma_{i+1}^y) \\ & + \sum_i J_{xz} (\sigma_i^x \sigma_{i+1}^z + \sigma_i^z \sigma_{i+1}^x) \\ & - \sum_i (\Gamma_z \sigma_i^z + \Gamma_x \sigma_i^x), \end{aligned} \quad (\text{B3})$$

where

$$J_x = \frac{A - B}{2} \cos(2\alpha) - C \sin(2\alpha) + \frac{A + B}{2} \quad (\text{B4})$$

$$J_z = -\frac{A - B}{2} \cos(2\alpha) + C \sin(2\alpha) + \frac{A + B}{2} \quad (\text{B5})$$

$$J_{xz} = \frac{A - B}{2} \sin(2\alpha) + C \cos(2\alpha) \quad (\text{B6})$$

$$\Gamma_z = (h_{ex}^z + 2B) \cos(\alpha) + 2C \sin(\alpha) \quad (\text{B7})$$

$$\Gamma_x = -(h_{ex}^z + 2B) \sin(\alpha) + 2C \cos(\alpha) \quad (\text{B8})$$

Let  $J_{xz} = 0$ , we can solve for  $\alpha$  such that the  $\sigma_i^x \sigma_{i+1}^z + \sigma_i^z \sigma_{i+1}^x$  terms are eliminated. The solution is given by  $\tan(2\alpha) = 2C/(B - A)$  if  $\theta \neq \arcsin(2/3)$  or  $(\alpha = \pi/4, \theta = \arcsin(2/3))$ , where  $\theta = \arcsin(2/3)$  is the angle for  $A = B$ . Notice that arctan function takes values between  $-\pi/2$  and  $\pi/2$ , there is a discontinuity when  $B - A$  becomes negative from positive as we increase  $\theta$ . We can let  $\alpha \in [0, \pi/2]$ , then we obtain an express of  $\alpha$  as a function of  $\theta$  in Eq. (14).

### Appendix C: Effects of odd and even number of sites

On the boundary sites, because the interaction only comes from one side in the bulk, they often prefer some particular states favored by the external field. For the AFM transition near the circle in our phase diagram, if we have even number of sites, the AFM state will have opposite spin states on the boundary sites. This is not favored by an uniform external field, then a state with a domain wall in the center may exist near the phase transition. Figure 8(a) shows that there exists a high entanglement plateau before the transition into the AFM phase, which is due to the domain-wall state that introduces a large entanglement constant. The constant will not scale with the system size, so it will not change the critical point. This high plateau may overwhelm the entanglement scaling at small system sizes, so we use odd number of sites to remove the domain-wall state. In the domain-wall state, there is a reflection symmetry, each half of the chain has a nonzero staggered order, but the staggered order is zero for the whole system. One can see from Fig. 8(b) that the circle of nonzero staggered order is smaller than the one for odd number of sites  $N = 257$  shown in Fig. 6. Figure 8(c) shows the AFM state with a domain wall at  $\theta = 0.42\pi, h^z = 1.0$  on the yellow entanglement plateau.

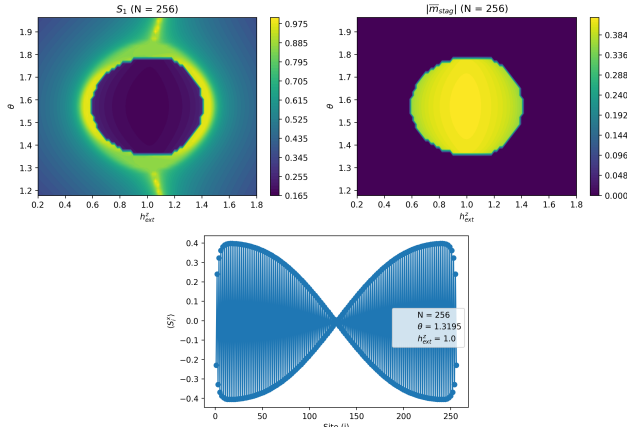


FIG. 8. Results for even number of sites  $N = 256$ . Upper left: Contour plot for the entanglement entropy. Upper right: Contour plot for the magnitude of the stagger magnetization vector. Lower: Spin density profile at  $\theta = 0.42\pi, h^z = 1.0$  on the yellow entanglement plateau.

### Appendix D: Finding critical points from peaks of entanglement entropy

For each system size, we calculate the entanglement entropy  $S_{\text{vN}}$  around the peak with a small step size  $\Delta h^z = 0.001$ , as shown in Fig. 9. We then use spline interpolation to find the peak position of  $S_{\text{vN}}$  with high accuracy. We fit the peak positions with a high degrees of polynomial to extrapolate the critical point in the thermodynamic limit. This is very accurate for Ising transitions because the correlation length exponent  $\nu = 1$ .

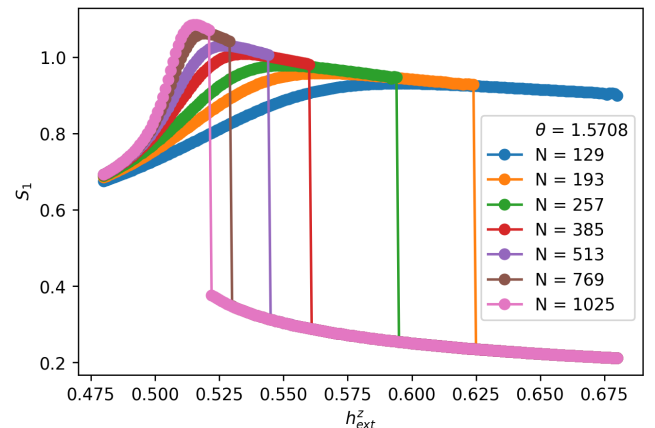


FIG. 9. Entanglement entropy  $S_{\text{vN}}$  as a function of  $h^z$  for different system sizes at  $\theta = \pi/2$ . The high entanglement plateau right to the peak in the phase diagram with  $N = 257$  in Fig. 1 recedes as  $N$  increases.

---

[1] D. D. Awschalom, N. Samarth, and D. Loss, eds., *Semiconductor Spintronics and Quantum Computation* (Springer Verlag, Heidelberg, 2002).  
[2] C. P. Anderson, E. O. Glen, C. Zeledon, A. Bourassa, Y. Jin, Y. Zhu, C. Vorwerk, A. L. Crook, H. Abe, J. Ul-Hassan, T. Ohshima, N. T. Son, G. Galli, and D. D. Awschalom, *Science Advances* **8**, eabm5912 (2022), <https://www.science.org/doi/10.1126/sciadv.abm5912>.  
[3] R. Schirhagl, K. Chang, M. Loretz, and C. L. Degen, *Annual Review of Physical Chemistry* **65**, 83 (2014).  
[4] D. D. Awschalom, R. Hanson, J. Wrachtrup, and B. B. Zhou, *Nature Photonics* **12**, 516 (2018).  
[5] E. Altman, K. R. Brown, G. Carleo, L. D. Carr, E. Demler, C. Chin, B. DeMarco, S. E. Economou, M. A. Eriks-

son, K.-M. C. Fu, M. Greiner, K. R. Hazzard, R. G. Hulet, A. J. Kollár, B. L. Lev, M. D. Lukin, R. Ma, X. Mi, S. Misra, C. Monroe, K. Murch, Z. Nazario, K.-K. Ni, A. C. Potter, P. Roushan, M. Saffman, M. Schleier-Smith, I. Siddiqi, R. Simmonds, M. Singh, I. Spielman, K. Temme, D. S. Weiss, J. Vučković, V. Vuletić, J. Ye, and M. Zwierlein, *PRX Quantum* **2**, 017003 (2021).

[6] D. R. Candido, G. D. Fuchs, E. Johnston-Halperin, and M. E. Flatté, *Mat. Quantum Technol.* **1**, 011001 (2021).

[7] J. M. Taylor, P. Cappellaro, L. Childress, L. Jiang, D. Budker, P. R. Hemmer, A. Yacoby, R. Walsworth, and M. D. Lukin, *Nat. Phys.* **4**, 810 (2008).

[8] P. M. Koenraad and M. E. Flatté, *Nature Materials* **10**, 91 (2011).

[9] F. Dolde et al., *Nature Physics* **7**, 459 (2011).

[10] F. Dolde, M. W. Doherty, J. Michl, I. Jakobi, B. Naydenov, S. Pezzagna, J. Meijer, P. Neumann, F. Jelezko, N. B. Manson, and J. Wrachtrup, *Phys. Rev. Lett.* **112**, 097603 (2014).

[11] R. Schirhagl, K. Chang, M. Loretz, and C. L. Degen, *Annual Review of Physical Chemistry* **65**, 83 (2014).

[12] T. van der Sar, F. Casola, R. Walsworth, and A. Yacoby, *Nat. Commun.* **6**, 7886 (2015).

[13] C. L. Degen, F. Reinhard, and P. Cappellaro, *Rev. Mod. Phys.* **89**, 035002 (2017).

[14] B. Flebus and Y. Tserkovnyak, *Phys. Rev. Lett.* **121**, 187204 (2018).

[15] F. Casola, T. van der Sar, and A. Yacoby, *Nat. Rev. Mater.* **3**, 17088 (2018).

[16] T. Mittiga, S. Hsieh, C. Zu, B. Kobrin, F. Machado, P. Bhattacharyya, N. Z. Rui, A. Jarmola, S. Choi, D. Budker, and N. Y. Yao, *Phys. Rev. Lett.* **121**, 246402 (2018).

[17] B. B. Zhou, P. C. Jerger, K.-H. Lee, M. Fukami, F. Mujid, J. Park, and D. D. Awschalom, *Phys. Rev. X* **10**, 011003 (2020).

[18] E. Lee-Wong, R. Xue, F. Ye, A. Kreisel, T. van der Sar, A. Yacoby, and C. R. Du, *Nano Letters* **20**, 3284 (2020).

[19] A. Rustagi, I. Bertelli, T. van der Sar, and P. Upadhyaya, *Phys. Rev. B* **102**, 220403(R) (2020).

[20] J. F. Barry, J. M. Schloss, E. Bauch, M. J. Turner, C. A. Hart, L. M. Pham, and R. L. Walsworth, *Rev. Mod. Phys.* **92**, 015004 (2020).

[21] J. Choi, S. Choi, G. Kucsko, P. C. Maurer, B. J. Shields, H. Sumiya, S. Onoda, J. Isoya, E. Demler, F. Jelezko, N. Y. Yao, and M. D. Lukin, *Phys. Rev. Lett.* **118**, 093601 (2017).

[22] G. Kucsko, S. Choi, J. Choi, P. C. Maurer, H. Zhou, R. Landig, H. Sumiya, S. Onoda, J. Isoya, F. Jelezko, E. Demler, N. Y. Yao, and M. D. Lukin, *Phys. Rev. Lett.* **121**, 023601 (2018).

[23] E. J. Davis, B. Ye, F. Machado, S. A. Meynell, T. Mittiga, W. Schenken, M. Joos, B. Kobrin, Y. Lyu, D. Bluvstein, et al., arXiv:2103.12742 (2021).

[24] B. L. Dwyer, L. V. Rodgers, E. K. Urbach, D. Bluvstein, S. Sangtawesin, H. Zhou, Y. Nassab, M. Fitzpatrick, Z. Yuan, K. De Greve, et al., arXiv:2103.12757 (2021).

[25] D. R. Candido and M. E. Flatté, arXiv preprint arXiv:2112.15581 (2021).

[26] M. W. Doherty, N. B. Manson, P. Delaney, F. Jelezko, J. Wrachtrup, and L. C. Hollenberg, *Physics Reports* **528**, 1 (2013), the nitrogen-vacancy colour centre in diamond.

[27] A. M. Edmonds, M. E. Newton, P. M. Martineau, D. J. Twitchen, and S. D. Williams, *Phys. Rev. B* **77**, 245205 (2008).

[28] B. L. Green, S. Mottishaw, B. G. Breeze, A. M. Edmonds, U. F. S. D’Haenens-Johansson, M. W. Doherty, S. D. Williams, D. J. Twitchen, and M. E. Newton, *Phys. Rev. Lett.* **119**, 096402 (2017).

[29] B. C. Rose, D. Huang, Z.-H. Zhang, P. Stevenson, A. M. Tyryshkin, S. Sangtawesin, S. Srinivasan, L. Loudin, M. L. Markham, A. M. Edmonds, D. J. Twitchen, S. A. Lyon, and N. P. de Leon, *Science* **361**, 60 (2018), <https://www.science.org/doi/pdf/10.1126/science.aa00290>.

[30] L. J. Rogers, K. D. Jahnke, M. H. Metsch, A. Sipahigil, J. M. Binder, T. Teraji, H. Sumiya, J. Isoya, M. D. Lukin, P. Hemmer, and F. Jelezko, *Phys. Rev. Lett.* **113**, 263602 (2014).

[31] W. F. Koehl, B. B. Buckley, F. J. Heremans, G. Calusine, and D. D. Awschalom, *Nature* **479**, 84 (2011).

[32] H. Seo, A. L. Falk, P. V. Klimov, K. C. Miao, G. Galli, and D. D. Awschalom, *Nature Communications* **7** (2016), 10.1038/ncomms12935.

[33] C. P. Anderson, A. Bourassa, K. C. Miao, G. Wolfowicz, P. J. Mintun, A. L. Crook, H. Abe, J. U. Hassan, N. T. Son, T. Ohshima, and D. D. Awschalom, *Science* **366**, 1225 (2019), <https://www.science.org/doi/pdf/10.1126/science.aax9406>.

[34] D. R. Candido and M. E. Flatté, *PRX Quantum* **2**, 040310 (2021).

[35] J. C. Lee, D. O. Bracher, S. Cui, K. Ohno, C. A. McLellan, X. Zhang, P. Andrich, B. Alemán, K. J. Russell, A. P. Magyar, I. Aharonovich, A. Bleszynski Jayich, D. Awschalom, and E. L. Hu, *Applied Physics Letters* **105**, 261101 (2014), <https://doi.org/10.1063/1.4904909>.

[36] C. A. McLellan, B. A. Myers, S. Kraemer, K. Ohno, D. D. Awschalom, and A. C. Bleszynski Jayich, *Nano Letters* **16**, 2450 (2016), pMID: 27010642, <https://doi.org/10.1021/acs.nanolett.5b05304>.

[37] P. Spinicelli, A. Dréau, L. Rondin, F. Silva, J. Achard, S. Xavier, S. Bansropun, T. Debuisschert, S. Pezzagna, J. Meijer, V. Jacques, and J.-F. Roch, *New Journal of Physics* **13**, 025014 (2011).

[38] D. M. Toyli, C. D. Weis, G. D. Fuchs, T. Schenkel, and D. D. Awschalom, *Nano Letters* **10**, 3168 (2010), pMID: 20698632, <https://doi.org/10.1021/nl102066q>.

[39] D. M. Toyli, C. D. Weis, G. D. Fuchs, T. Schenkel, and D. D. Awschalom, *Nano Letters* **10**, 3168 (2010).

[40] C. J. Stephen, B. L. Green, Y. N. D. Lekhai, L. Weng, P. Hill, S. Johnson, A. C. Frangeskou, P. L. Diggle, Y.-C. Chen, M. J. Strain, E. Gu, M. E. Newton, J. M. Smith, P. S. Salter, and G. W. Morley, *Phys. Rev. Applied* **12**, 064005 (2019).

[41] V. L. Pokrovsky and A. L. Talapov, *Phys. Rev. Lett.* **42**, 65 (1979).

[42] V. R. Kortan, C. Şahin, and M. E. Flatté, *Phys. Rev. B* **93**, 220402(R) (2016).

[43] C. S. Ho, S. G. Tan, M. B. A. Jalil, Z. Chen, and L. A. Krivitsky, *Phys. Rev. B* **94**, 245424 (2016).

[44] J. D. A. Wood, D. A. Broadway, L. T. Hall, A. Stacey, D. A. Simpson, J.-P. Tetienne, and L. C. L. Hollenberg, *Phys. Rev. B* **94**, 155402 (2016).

[45] M. Auzinsh, A. Berzins, D. Budker, L. Busaite, R. Ferber, F. Gahbauer, R. Lazda, A. Wickenbrock, and H. Zheng, *Phys. Rev. B* **100**, 075204 (2019).

[46] S. R. White, *Phys. Rev. Lett.* **69**, 2863 (1992).

- [47] S. R. White, Phys. Rev. B **48**, 10345 (1993).
- [48] S. Östlund and S. Rommer, Phys. Rev. Lett. **75**, 3537 (1995).
- [49] M. Fishman, S. R. White, and E. M. Stoudenmire, Sci. Post Phys. Codebases , 4 (2022).
- [50] C. Holzhey, F. Larsen, and F. Wilczek, Nuclear Physics B **424**, 443 (1994).
- [51] G. Vidal, J. I. Latorre, E. Rico, and A. Kitaev, Phys. Rev. Lett. **90**, 227902 (2003).
- [52] A. Langari, Phys. Rev. B **58**, 14467 (1998).
- [53] C. N. Yang and C. P. Yang, Phys. Rev. **150**, 321 (1966).
- [54] A. Dutta and D. Sen, Phys. Rev. B **67**, 094435 (2003).
- [55] N. Chepiga and F. Mila, Phys. Rev. Lett. **122**, 017205 (2019).
- [56] A. Lazarides, O. Tielemans, and C. Morais Smith, Phys. Rev. B **80**, 245418 (2009).
- [57] S. Nyckees and F. Mila, Phys. Rev. Research **4**, 013093 (2022).
- [58] N. Chepiga and F. Mila, Nature Communications **12**, 414 (2021).
- [59] A. Keesling, A. Omran, H. Levine, H. Bernien, H. Pichler, S. Choi, R. Samajdar, S. Schwartz, P. Silvi, S. Sachdev, P. Zoller, M. Endres, M. Greiner, V. Vuletić, and M. D. Lukin, Nature **568**, 207 (2019).
- [60] H. Zou, Y. Liu, C.-Y. Lai, J. Unmuth-Yockey, L.-P. Yang, A. Bazavov, Z. Y. Xie, T. Xiang, S. Chandrasekharan, S.-W. Tsai, and Y. Meurice, Phys. Rev. A **90**, 063603 (2014).
- [61] J. Unmuth-Yockey, J. Zhang, P. M. Preiss, L.-P. Yang, S.-W. Tsai, and Y. Meurice, Phys. Rev. A **96**, 023603 (2017).
- [62] A. Bazavov, Y. Meurice, S.-W. Tsai, J. Unmuth-Yockey, and J. Zhang, Phys. Rev. D **92**, 076003 (2015).
- [63] J. Zhang, J. Unmuth-Yockey, J. Zeiher, A. Bazavov, S.-W. Tsai, and Y. Meurice, Phys. Rev. Lett. **121**, 223201 (2018).
- [64] J. Unmuth-Yockey, J. Zhang, A. Bazavov, Y. Meurice, and S.-W. Tsai, Phys. Rev. D **98**, 094511 (2018).
- [65] J. Zhang, Y. Meurice, and S.-W. Tsai, Phys. Rev. B **103**, 245137 (2021).
- [66] J. Zhang, Phys. Rev. B **104**, 205112 (2021).